Mercury isotopic compositions in fine particles and offshore surface seawater in a coastal area of East China: Implication for Hg sources and atmospheric transformations

Lingling Xu[a,b,*], Jiayan Shi[b,d], Yuping Chen[a,b,c], Yanru Zhang[a,b,c], Mengrong Yang[a,b], Yanting Chen[a,b], Liqian Yin[a,b], Lei Tong[a,b], Hang Xiao[a,b], Jinsheng Chen[a,b,*]

[a] *Center for Excellence in Regional Atmospheric Environment, Institute of Urban Environment, Chinese Academy of Sciences, Xiamen 361021, China*

[b] *Key Lab of Urban Environment and Health, Institute of Urban Environment, Chinese Academy of Sciences, Xiamen 361021, China*

[c] *University of Chinese Academy Sciences, Beijing 100049, China*

[d] *College of Resources and Environment, Fujian Agriculture and Forestry University, Fuzhou 350002, China*

* Corresponding author.

E-mail address: jschen@iue.ac.cn (J.S. Chen); linglingxu@iue.ac.cn (L.L. Xu)

30 **Abstract.** Isotopic compositions of Hg in atmospheric particles (Hg$_{PM}$) are probably

31 the mixed results of emission sources and atmospheric processes. Here, we present Hg

32 isotopic compositions in daily fine particles (PM$_{2.5}$) collected from an industrial site

33 (CX) and a nearby mountain site (DMS) in a coastal area of East China, as well as in

34 surface seawater close to the industrial area, to reveal the influence of anthropogenic

35 emission sources and atmospheric transformations on Hg isotopes. The PM$_{2.5}$ samples

36 displayed a significant spatial difference in δ^{202}Hg. For the CX, the negative δ^{202}Hg

37 values are similar to those of source materials and the Hg$_{PM}$ contents were well

38 correlated with chemical tracers, indicating the dominant contributions of local

39 industrial activities to Hg$_{PM2.5}$. Whereas the observed positive δ^{202}Hg at the DMS was

40 likely associated with regional emissions and extended atmospheric processes during

41 transport. The Δ^{199}Hg values in PM$_{2.5}$ from the CX and DMS were comparable

42 positive. The unity slope of Δ^{199}Hg versus Δ^{201}Hg over all data suggests that the

43 odd-MIF of Hg$_{PM2.5}$ was primarily induced by photo-reduction of Hg^{2+} in aerosols.

44 The positive Δ^{200}Hg values with a minor spatial difference were probably associated

45 with photo-oxidation of Hg^0 which is generally enhanced in the coastal environment.

46 Total Hg in offshore surface seawater was characterized by negative δ^{202}Hg and

47 near-zero Δ^{199}Hg and Δ^{200}Hg values, which are indistinguishable from Hg isotopes of

48 source materials. Overall, the PM$_{2.5}$ collected from industrial areas had comparable

49 δ^{202}Hg values but more positive Δ^{199}Hg and Δ^{200}Hg as compared to surface seawater.

50 The results indicate that atmospheric transformations would induce significant

51 fractionation of Hg isotopes and obscure the Hg isotopic signatures of anthropogenic

52 emissions.

53

54 *Keywords:* Particle bound mercury; Surface seawater; Hg isotopes; Mercury sources;

55 Photo-chemical processes.

56

57

58

59

1. Introduction

Mercury (Hg) is a genotoxic element and was ranked with the priority controlled pollutants in many countries. Atmospheric Hg was operationally defined as three forms: gaseous elemental mercury (GEM), gaseous oxidized mercury (GOM), and particle bound mercury (PBM or Hg_{PM}) (Schroeder and Munthe, 1998). Previous studies indicated that Hg_{PM} concentrations in urban and industrial areas could reach up to hundreds even thousands of pg m^{-3}, relative to tens of pg m^{-3} in uncontaminated remote areas (Fu et al., 2015; Mao et al., 2016). In addition, Hg_{PM} can account for up to 40% of atmospheric Hg in industrial areas, relative to < 5% in uncontaminated areas (Guo et al., 2022;Schroeder and Munthe, 1998). Hence, particulate matter (PM) can act as a vector of toxic Hg and inhalation of Hg-carrying particles is an important pathway of human exposure to atmospheric Hg. Coal combustion, non-ferrous metal smelting, and cement production were the three primary anthropogenic sources of atmospheric Hg, which are responsible for 47% of total global Hg emissions (GMA, 2018). On the other hand, Hg_{PM} undergoes complex transport and transformation processes in the atmosphere. Hg_{PM} can be formed by uptake of GOM in particles, which made an important contribution to Hg_{PM} in the heavily particle polluted areas (Xu et al., 2020). Whereas reduction of GOM binding with dissolved organic carbon ligands in aqueous particles potentially converts it back to the gas phase (Horowitz et al., 2017). In addition, Hg_{PM} has a residence time of several weeks as it can transport and deposit at a regional scale (Selin, 2009). The research has suggested that atmospheric Hg_{PM} is generally a combined result of anthropogenic emissions andatmospheric processes, which plays a crucial role in the global cycling of Hg.

Analysis technique of Hg isotopes and mechanisms of Hg isotopic fractionation have come a long way in the last decade (Blum and Johnson, 2017). Hg has seven stable isotopes (including ^{196}Hg, ^{198}Hg, ^{199}Hg, ^{200}Hg, ^{201}Hg, ^{202}Hg, and ^{204}Hg) and exhibits mass dependent fractionation (MDF) and mass independent fractionation (MIF) in various environmental samples and processes (Blum and Johnson, 2017;Sonke and Blum, 2013; Yin et al., 2014a). MDF of Hg isotopes is often reported as $\delta^{202}Hg$, while MIF of odd mass-numbered Hg isotopes (odd-MIF) is reported as

90   $\Delta^{199}Hg$ and $\Delta^{201}Hg$ and MIF of even Hg isotopes (even-MIF) as $\Delta^{200}Hg$ and $\Delta^{204}Hg$.

91   Previous laboratory and field studies have revealed that nearly all biogeochemical

92   processes induce MDF of Hg isotopes, whereas significant odd-MIF of Hg occurs

93   mainly in photochemical processes (Bergquist and Blum, 2007; Blum et al., 2014;

94   Malinovsky et al., 2010; Sun et al., 2016a). What's more, specific ratios of

95   $\Delta^{199}Hg/\Delta^{201}Hg$ have been reported for different transformation processes, i.e., ~1.0 for

96   photo-reduction of Hg^{2+} and ~1.6 for photo-oxidation of Hg^0 (Bergquist and Blum,

97   2007; Sun et al., 2016a). Even-MIF of Hg isotopes is observed mostly in atmosphere

98   related samples, which is suggested to associate with photo-oxidation of Hg^0 by UV

99   and oxidants (Blum and Johnson, 2017; Chen et al., 2012; Fu et al., 2019). Therefore,

100 Hg isotopes are capable of becoming useful tracers for the biogeochemical cycles of

101 Hg in the environment.

102 There is a large difficulty in sampling enough Hg mass for analyzing Hg isotopes

103 of atmospheric samples. Even so, a few public studies have proved that Hg isotopes

104 are useful tools to investigate potential sources and transformation processes of Hg in

105 the atmosphere. The PM from major cities, like in northern and western China, mostly

106 displayed significant negative MDF and near zero odd-MIF due to the dominant

107 impact of anthropogenic emissions (Huang et al., 2015, 2016, 2019, 2020; Xu et al.,

108 2017, 2019;Yu et al., 2016). A previous study conducted in remote areas of China has

109 reported that the Hg_{PM} exposed to air masses of regional and long-range sources had

110 distinct isotopic signatures (Fu et al., 2019). Recently, many studies have used Hg

111 isotopes to investigate the contribution of domestic emissions and transboundary Hg

112 transport to atmospheric Hg_{PM}. These studies have implied that the long-range

113 transboundary Hg transport from South Asia played a crucial role in the Himalayas

114 and the Tibetan Plateau, even in the southwestern and northwestern China (Fu et al.,

115 2019; Guo et al., 2021, 2022). East China is densely populated and one of the heaviest

116 industrialized area in China. The concentration of Hg_{PM} in this region has been well

117 characterized (Hong et al., 2016; Xu et al., 2020;Yu et al., 2015), but only two studies

118 conducted at the remote sites have referred to Hg_{PM} isotopes (Fu et al., 2019;Yu et al.,

119 2016). To the best of our knowledge, there is no report on the isotopic compositions of

120 Hg_{PM} from urban areas of East China. Likewise, the effect of atmospheric processes

121 on the fractionation of Hg isotopes in the coastal region has not been well elucidated.

122 This study determined Hg isotopic compositions in $PM_{2.5}$ collected from an

123 industrial site and a mountain site in a coastal area of East China. Comparison of

124 $Hg_{PM2.5}$ isotopes at the neighboring sites would eliminate the impacts of meteorology

125 and atmospheric Hg background which vary across space on Hg_{PM} isotopes.

126 Furthermore, this study measured the isotopic compositions of total mercury (THg) in

127 surface seawater close to the industrial area and distinguished Hg isotopes between

128 the atmospheric sample and surface medias. The objectives of this study are (1) to

129 differentiate the Hg isotopes in $PM_{2.5}$ from the two neighboring industrial and

130 mountain sites; (2) use the Hg isotopes to explore the influence of anthropogenic

131 sources on the Hg_{PM}; (3) to reveal the role of atmospheric transformations in varying

132 Hg_{PM} isotopic compositions.

133 **2. Experiment**

134 *2.1. Study area description*

135 $PM_{2.5}$ sampling was conducted at an industrial site (Chunxiao, CX) and a nearby

136 mountain site (Daimeishan, DMS) on the east coast of Zhejiang province, East China

137 (Fig. 1). The study region experiences a typical subtropical monsoon climate, with sea

138 breeze in summer and continental breeze in winter. The average annual temperature,

139 precipitation, relative humidity, and sunshine hours were 18.1 °C, 1608 mm, 76.8%,

140 and 1797 h, respectively.

141 The CX (121.91 ° E, 29.87 ° N, 15 m a.g.l.) is located in the Urban Environment

142 Observation and Research Station, Chinese Academy of Sciences, Beilun District,

143 Ningbo. Ningbo is a highly industrial city and there is a high density of industrial

144 activities around the CX. Potential Hg point sources include a large coal-fired power

145 plant (5000 MW) approximately 20 km to the northwest, a Chlor-alkali plant 20 km to

146 the northeast, and an automobile assembly plant within 1 km of the site. The CX is in

147 close proximity to the East China Sea (ECS, ~ 0.6 km), thus clean air masses from the

148 sea in warm seasons would dilute atmospheric Hg at the CX. The DMS (121.62 ° E,

149 29.68 ° N, 450 m a.s.l.) is located at the summit of Mountain Damei, which is

150   surrounded by trees. The site is 20 km to the coast of the ECS and approximately 22

151   km south of Ningbo. There are no significant Hg point sources within a radius of ~10

152   km from the DMS. However, an early study reported that intense regional emissions,

153   like industrial activities and coal combustion in the Yangtze River Delta and the

154   neighboring region of Anhui, Jiangsu, and Zhejiang Provinces, caused a high

155   atmospheric Hg concentration at the DMS (Yu et al., 2015).

156   Surface seawater samples were collected in the offshore area of Ningbo. The

157   seawater sampling area (about 122.04 °E, 29.82 °N, Fig. 1) is approximately 1 km

158   west of the Beilun District, Ningbo. The salinity of the seawater samples ranged from

159   21.2‰ to 29.5‰. The pH of the seawater samples was in the range of 5.7 ~ 8.5, with

160   the mean value of 7.5 ±0.6.
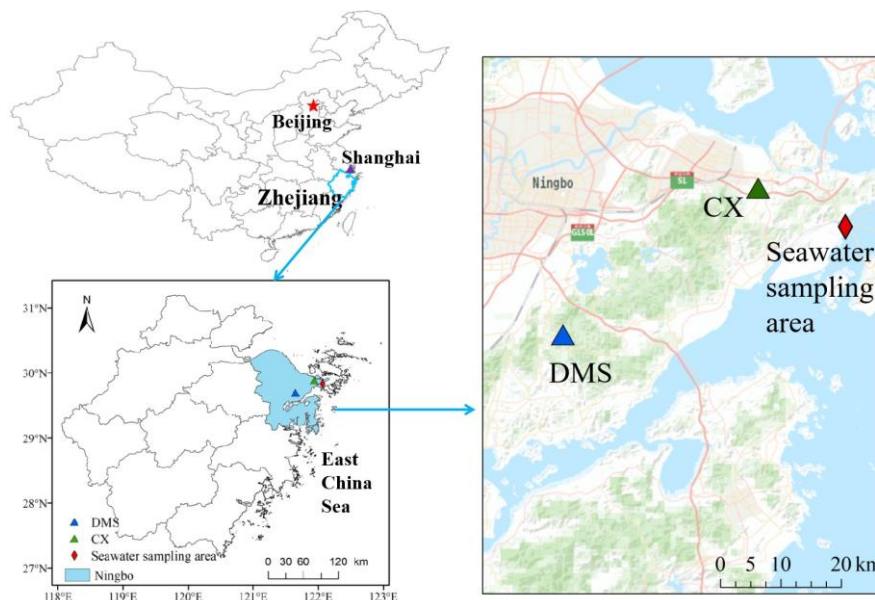
161

162   **Fig. 1**   Locations of PM$_{2.5}$ (CX: industrial site; DMS: mountain site) and surface
163   seawater sampling area.

164   *2.2. Sample collection and analysis*

165   *2.2.1. Sampling of PM$_{2.5}$*

166   The period of PM$_{2.5}$ sampling was from Jul. 2017 to Jun. 2018. Daily PM$_{2.5}$

167   samples were collected 1~2 times a week at the CX (except Jan. and Feb. 2018) and

168   once a week at the DMS. Field blank samples were collected at each site. PM$_{2.5}$

169   samples were collected on a preheated quartz-fiber filter (500 °C, 4 h, 8 × 10 inches,

170   Whatman) using a high volume sampler (Tianhong TH1000H, China) with a flow rate

171   of 1.05 m³ min⁻¹. The filters were conditioned at $24 \pm 1\ ^{\circ}\text{C}$ and $52 \pm 2\%$. The mass

172   loading of $PM_{2.5}$ on filters was determined by mass difference before and after

173   sampling. The filter samples were wrapped in aluminum foils and stored at -20 ℃

174   until analysis.

175   *2.2.2. Concentration of Hg and other chemical species in $PM_{2.5}$*

176   Six punches (ca. 0.5 cm² per punch) of each sampling filter were digested by a

177   10 mL of 40% aqua regia (HNO_3: HCl = 1:3, *v/v*) in a water bath at 95 ℃ for 5 min,

178   then the solution was oxidized by 1 mL of 0.2 M BrCl and bathed for another 30 min.

179   After cooling down, the extracted solution was diluted to 15 mL with ultra-pure water

180   and then analyzed by cold-vapor atomic fluorescence spectrometry (CVAFS, Brooks

181   Rand Model III, USA) following the EPA method 1631. The content of Hg on blank

182   filters can be negligible (42.5 pg at the CX and 27.0 pg at the DMS) relative to those

183   on sample filters.

184    $PM_{2.5}$ samples selected for Hg isotopes analysis were also measured for 8 water

185   soluble inorganic ions (K^+, Ca^{2+}, Na^+, Mg^{2+}, Cl^-, SO_4^{2-}, NO_3^-, and NH_4^+), elemental

186   carbon (EC), organic carbon (OC), and levoglucosan. The water soluble ions were

187   analyzed by ion chromatography (ICS-3000, Dionex, USA). EC and OC were

188   analyzed using a carbon analyzer (Model 4, Sunset Lab., USA) and NOISH protocol.

189   Analytical procedures and quality control procedures have been described by Xu et al.

190   (2018). Levoglucosan, an excellent indicator of biomass burning, was analyzed using

191   a gas chromatography‐mass spectrometer detector (GC‐MS, Agilent 7890A-5975C,

192   Agilent Tech. Inc., USA). Levoglucosan analytical procedures have been presented in

193   detail elsewhere (Hong et al., 2019).

194   *2.2.3. Sampling and analysis of Hg in seawater*

195   Seawater samples were collected from the surface of the offshore sampling area

196   twice a month during Jul. 2017 ~ Jun. 2018, except Feb. 2018. Each time, three ~50

197   mL of duplicate seawater samples were collected for THg content analysis. Final THg

198   content was determined by the average of three duplicate samples. In addition, ~2 L

199   surface seawater was sampled for Hg isotopes analysis each time. The seawater

200   samples were stored in brown glass bottles and preserved with 1% (*v/v*) HCl in the

201 laboratory. They were analyzed for Hg content and isotopic compositions in a month.

202   Total Hg content in seawater samples was measured by CVAFS (Brooks Rand

203 Model III, USA). A 25 mL of seawater sample was digested with 0.2 M BrCl at least

204 12 h in advance and then analyzed using the EPA method 1631. More details can be

205 found in a previous study (Xu et al., 2014). Method blank was processed by bottles

206 filling up with ultra-pure water instead of seawater. The blank was lower than 10 pg

207 (n = 15), which can be negligible compared to the samples.

208 *2.3. Analysis of Hg isotopic compositions*

209 *2.3.1. $PM_{2.5}$ sample processing*

210   Due to the effects of precipitation and short sampling duration, the mass of Hg

211 on most of $PM_{2.5}$ samples was not sufficient for isotopes detection. A total of 20 $PM_{2.5}$

212 samples, including 10 at the CX and 10 at the DMS, were chosen for Hg isotopes

213 analysis. Pre-concentration of Hg from $PM_{2.5}$ samples was conducted following a

214 dual-stage combustion protocol (Huang et al., 2015). To be specific, a tube furnace

215 (OTF-1200X-Π, Kejin, China) consisting of two combustion stages was used. A

216 sampling filter was embedded in a furnace quartz tube (50 mm OD, 46 mm ID, 80 cm

217 length). The tube was then placed in the furnace so that the filter was at the first

218 combustion stage. The second decomposition stage was heated up in advance and

219 maintained at 1000 ℃, then the first combustion stage was heated up to 950 ℃

220 through a temperature-programmed procedure. The combustion procedure was run

221 with no samples in the furnace quartz tube before $PM_{2.5}$ sample treatment every day to

222 remove residual volatiles. The released Hg was transferred by O_2/Ar gas (30%/70%)

223 at a flow rate of 20 mL min^{-1} and then trapped by a 10 mL of 40% inverse aqua regia

224 (2: 4: 9 ratio of 10 M HCl, 15 M HNO_3 and ultra-pure water) in a designed glass

225 bottle. In advance of $PM_{2.5}$ sample analysis, the accuracy of dual-stage combustion

226 method was assessed by the analysis of the standard NIST SRM 3133 Hg (dripped on

227 blank filters) and the certified reference material GBW07434. The Hg recovery

228 efficiency of the dual-stage protocol was in the range of 87.6% ~ 103.3% (mean: 95.0

229 $\pm$ 5.1%, n = 6).

230 *2.3.2. Seawater sample processing*

231   A total of 20 seawater samples were analyzed for Hg isotopes. ~2 L seawater

232   sample was mixed with a 4 mL of 300 g L^{-1} NH$_2$OH HCl solution for neutralizing

233   excess BrCl and then an 8 mL of 200 g L^{-1} SnCl$_2$ solution for reducing the oxidized

234   Hg. The pre-treated seawater sample was stirred and bubbled for 1 h with Hg-free N$_2$

235   at a flow rate of 400 mL min^{-1}. The gaseous Hg purged off seawater samples was

236   collected by a series of three gold traps. The gold traps were heated and the released

237   Hg was transferred by Hg-free N$_2$ at 10~15 mL min^{-1} and concentrated by a 10 mL of

238   40% inverse aqua regia.

239   *2.3.3. Hg isotopes analysis*

240   All trapping solutions were preserved with 1% (*v/v*) BrCl and stored at 4 ℃ in

241   the dark before Hg isotopes analysis. Hg isotopic compositions were measured by a

242   multi–collector inductively coupled plasma mass spectrometer (MC-ICP-MS, Nu

243   Instruments Ltd. UK) equipped with an introduction device following the protocols

244   presented in previous studies (Huang et al., 2015; Huang et al., 2021;Lin et al., 2015).

245   The introduction device includes a modified cold-vapor generator (CVG) and an

246   Aridus III nebulizer for respective Hg and Tl introduction. Between standard and

247   sample, the CVG was rinsed with 3% (v/v) HNO$_3$ solution to ensure the Hg signal

248   returned to the background level. Instrument mass bias was corrected using both an

249   internal standard (NIST 997 Tl) and a strict sample-standard bracketing method

250   (NIST 3133 Hg). A reference material NIST 8610 was measured repeatedly for

251   quality control. The pre-concentration solutions were diluted to about 1.5 ~ 3.0 ng

252   mL^{-1} and the NIST 3133 and NIST 8610 were kept at 2.0 ng mL^{-1} during the analysis

253   period. The MDF of Hg (represented by δ-value, ‰) is defined by the following

254   equation (Blum and Bergquist, 2007):

255    $\delta^{xxx}Hg\ (‰) = [(^{xxx}Hg/^{198}Hg)_{sample}/(^{xxx}Hg/^{198}Hg)_{NIST\ 3133} -1] \times 1000$ (1)

256   where xxx = 199, 200, 201, and 202. The MIF of Hg (Δ-value, ‰) is calculated using

257   the theoretically predicted MDF as the following equation (Blum and Bergquist,

258   2007):

259    $\Delta^{xxx}Hg\ (‰) = \delta^{xxx}Hg - (\delta^{202}Hg \times \beta)$ (2)

260   where the mass-dependent scaling factor *β* is 0.252 for ^{199}Hg, 0.502 for ^{200}Hg, and

0.752 for [201]Hg. The repeated measurement of NIST 8610 during the analysis session yielded δ^{202}Hg and Δ^{199}Hg values of -0.60 ±0.15‰ and -0.02 ±0.06‰ (2σ, n = 7). In addition, a well-known reference material UM-Almaden showed a long-term average of δ^{202}Hg = -0.59 ±0.10‰ and Δ^{199}Hg = -0.03 ±0.07‰ (2σ, n = 25), which are well consistent with those in previous studies (Blum and Bergquist, 2007; Huang et al., 2015). The samples of this study were measured only once, so the 2σ uncertainties derived from repeated measurements of NIST 3133 standard during each analysis section were applied to the samples.

3. Results and discussion

3.1. Concentrations and isotopic compositions of Hg$_{PM2.5}$

Concentrations and isotopes of Hg$_{PM2.5}$ at industrial and mountain sites are showed in Table 1. Mean volumetric concentrations of Hg$_{PM2.5}$ were 16.3 ± 17.8 pg m^{-3} at the CX and 29.6 ± 35.9 pg m^{-3} at the DMS, which are comparable to those observed at remote sites (Fu et al., 2019), but lower than those reported from urban sites in China (Xu et al., 2019). The low volumetric concentrations of Hg$_{PM2.5}$ observed in this study were likely associated with low PM$_{2.5}$ concentrations (mean: 28.0 μg m^{-3} at the CX and 34.8 μg m^{-3} at the DMS) during the study period. Average mass concentrations of Hg$_{PM2.5}$ were 0.52 ± 0.23 μg g^{-1} (0.15 to 1.10, n = 51) at the CX and 0.85 ± 0.63 μg g^{-1} (0.18 to 2.80, n = 33) at the DMS, respectively. A relatively high concentration of Hg$_{PM2.5}$ has been reported at the DMS before, which was likely due to regional Hg emissions, mainly the industrial activities and coal combustion in the Yangtze River Delta and the neighboring region of Anhui, Jiangsu, and Zhejiang Provinces (Yu et al., 2015). The Hg contents in PM$_{2.5}$ of this study are higher than those of natural sources (e.g., dust and topsoil; 0.056 ~ 0.30 μg g^{-1}; Schleicher et al., 2015) and those of coals in China (mean: 0.22 μg g^{-1}; Yin et al., 2014b), which implies a potential contribution of anthropogenic sources with high Hg contents. The volumetric concentrations of Hg$_{PM2.5}$ were closely correlated to Hg$_{PM2.5}$/PM$_{2.5}$ ratios both at the CX and DMS (R^2 = 0.50 and 0.60, $p < 0.01$), suggesting that atmospheric Hg$_{PM2.5}$ concentrations were dependent on Hg contents. Whereas, a weak correlation between the Hg$_{PM2.5}$ volumetric concentrations and PM$_{2.5}$

masses was observed at the DMS ($R^2 = 0.25$, $p < 0.01$) in contrast to the CX ($R^2 = 0.77$, $p < 0.01$). The result likely indicates that the DMS $Hg_{PM2.5}$ was influenced by diverse sources of $PM_{2.5}$ with different Hg levels and/or complex atmospheric Hg transformations (Xu et al., 2019). This is supported by the higher variation coefficient (VC = SD/Mean) of $Hg_{PM2.5}$ mass concentrations at the DMS (74.1%) than the CX (44.2%). Spatial differences of $Hg_{PM2.5}$ were further examined by relationships of Hg with other chemical species in $PM_{2.5}$ (Table S1). In contrast to DMS, the mass concentrations of $Hg_{PM2.5}$ at the CX were well correlated to chemical tracers, like Cl^-, NO_3^-, K^+, and OC ($r = 0.40 \sim 0.57$, $p < 0.05$, Spearman correlation), implying the contributions of steady anthropogenic sources to $Hg_{PM2.5}$ in the industrial area.

$\delta^{202}Hg$ values for $Hg_{PM2.5}$ at the CX were in the range of -1.11‰ to 0.08‰ (mean: -0.61 ±0.35‰, n = 10), while $\delta^{202}Hg$ values at the DMS were significantly higher and in a larger variation from -0.78‰ to 1.10‰ (mean: 0.12 ±0.63‰, n = 10) ($p < 0.05$, T Test; Table 1 and Table S2). Hg_{PM} isotopic compositions in multiple types of locations are showed in Fig. 2 and Table S3. The $\delta^{202}Hg$ values at the CX basically overlap those for PM in urban areas of China (mean: from -1.60‰ to -0.42‰), as well as those for major source materials such as coal combustion, smelting, and cement plants (mean: -1.10‰, -0.87‰, and -1.42‰ respectively, Huang et al., 2016) and those for PM near anthropogenic emissions such as industry, landfill, traffic, and coal-fired power plants (mean: from -2.41‰ to -0.58‰) (Fig. 2). The result likely indicates an important contribution of anthropogenic sources to the CX $Hg_{PM2.5}$. However, the $\delta^{202}Hg$ values of above mentioned potential sources are not distinguishable, thus we could not identify the specific sources of $Hg_{PM2.5}$ solely based on Hg isotopes. On the other hand, the slight positive $\delta^{202}Hg$ values at the DMS are quite different from those observed at remote sites (mean: from -1.45‰ to -0.83‰; Fig. 2). Nevertheless, a less negative MDF of $Hg_{PM2.5}$ has also been reported at the DMS in a previous study ($\delta^{202}Hg$ = -0.26‰, Yu et al., 2016). Hg_{PM} from immediate anthropogenic emissions is generally characterized by negative $\delta^{202}Hg$, which in turn suggests that the more positive $\delta^{202}Hg$ of Hg_{PM} at the DMS might be affected by atmospheric processes, like photo-reduction of Hg^{2+} (Bergquist and Blum, 2007; Zheng and Hintelmann, 2009).

In contrast to MDF, the odd-MIF of $Hg_{PM2.5}$ at the two sites were comparable ($p > 0.05$, T Test), with $\Delta^{199}Hg$ values of $0.17 \pm 0.22‰$ (from -0.17‰ to 0.52‰) at the CX and $0.16 \pm 0.24‰$ (from -0.22‰ to 0.47‰) at the DMS, respectively. The significant positive $\Delta^{199}Hg$ in this study are similar to those observed in coastal areas (Rolison et al., 2013; Yu et al., 2020) and in remote areas in China (Fu et al., 2019), but distinguishable from those in urban and industrial areas with near-zero values due to anthropogenic emissions (Das et al., 2016; Huang et al., 2016, 2018, 2020; Xu et al., 2019; Yu et al., 2016). A laboratory study has indicated that photo-reduction of Hg^{2+} restrains odd Hg in reactants (aerosols here) in priority, which shifts $\Delta^{199}Hg$ values positively (Bergquist and Blum, 2007). Thus, it's reasonably supposed that the positive odd-MIF of Hg_{PM} in the study region was associated with photo-reduction of Hg^{2+} in aerosols. As shown in Table S2 and Fig. S1, PM2.5 samples affected by long range transport of air masses mostly had large positive $\Delta^{199}Hg$, like PM2.5 collected on Apr. 4, 2018 from the CX and on Jan. 10, 2018 from the DMS. It's probably related to extensive photo-reduction of Hg^{2+} in aerosols during long-range transport, as previous studies suggested (Fu et al., 2019; Huang et al., 2016). In addition, the MIF of ^{200}Hg, most probably relating to photo-reactions, was significant positive and displayed no spatial difference ($0.11 \pm 0.07‰$ at the CX and $0.14 \pm 0.07‰$ at the DMS; $p > 0.05$, T Test), which suggests enhanced and homogeneous photo-reactions in the study region. It is worth noting that a part of PM2.5 samples collected from the DMS displayed negative $\delta^{202}Hg$ and near-zero $\Delta^{199}Hg$, similar to those from the CX (Fig. 2). Compared with the previous study (Yu et al., 2016), our results provide isotopes evidence that $Hg_{PM2.5}$ at the DMS was affected by multiple sources and one of them might be regional anthropogenic emissions.

Table 1 Concentrations and isotopic compositions of $Hg_{PM2.5}$ at the industrial site (CX) and mountain site (DMS) in East China

Parameter [a]	CX		DMS	
	Mean $\pm$ sd	Range	Mean $\pm$ sd	Range
$Hg_{PM2.5}$ ($\mu g\ g^{-1}$)	0.52 ± 0.23	$0.15 \sim 1.10$	0.85 ± 0.63	$0.18 \sim 2.80$
$Hg_{PM2.5}$ ($pg\ m^{-3}$)	16.3 ± 17.8	$1.6 \sim 90.7$	29.6 ± 35.9	$2.9 \sim 181.3$
$\delta^{202}Hg$ (‰)	-0.61 ± 0.35	$-1.11 \sim 0.08$	0.12 ± 0.63	$-0.78 \sim 1.10$

Δ^{199}Hg (‰)	0.17 ±0.22	-0.17 ~ 0.52	0.16 ±0.24	-0.22 ~ 0.47
Δ^{201}Hg (‰)	0.21 ±0.18	-0.07 ~ 0.48	0.23 ±0.36	-0.29 ~ 0.66
Δ^{200}Hg (‰)	0.11 ±0.07	-0.01 ~ 0.23	0.14 ±0.07	0.06 ~ 0.28
Δ^{204}Hg (‰)	0.19 ±0.36	-0.16 ~ 0.93	3.58 ±3.68	0.26 ~ 11.38

347 [a] 51 samples collected from CX and 32 samples from DMS were used for $Hg_{PM2.5}$ concentration

348 analysis; 10 samples from each site for isotope analysis.
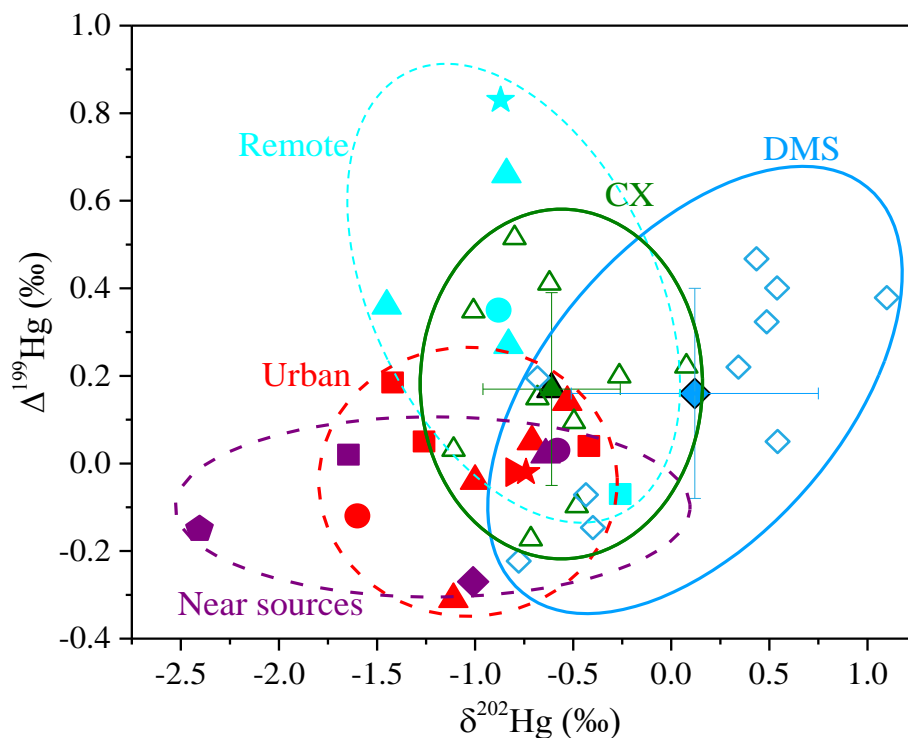
349

350 **Fig. 2** Isotopic compositions of Hg_{PM} at the multiple types of sites

351 (This study: ▲△mean and each values at the CX, ◆◇mean and each values at the DMS;

352 Remote sites: ★coast, ■▲mountain, ●island (Fu et al., 2019; Rolison et al., 2013; Yu et al.,

353 2016); Urban sites in China: ▲Beijing, ●Changchun, ★Chengdu, ■Guiyang, ▶Xi'an (Huang

354 et al., 2015, 2016, 2019, 2020; Xu et al., 2017, 2019; Yu et al., 2016); Sites near emission sources:

355 ▲■industrial, ●landfill, ◆traffic, ★near CFPP (Das et al., 2016; Huang et al., 2018; Yu et al.,

356 2016)

357 ***3.2. Influence of anthropogenic emissions on MDF of $Hg_{PM2.5}$***

358 Prior studies have compiled Hg isotopic compositions of major source materials,

359 such as fossil fuels, non-ferrous metal ores, and crustal rocks, which generally display

360 large negative δ^{202}Hg and negative or near-zero Δ^{199}Hg values (Huang et al., 2016;

361 Sun et al., 2016b). Combustion or/and industrial processing induces limited MIF (Sun

362 et al., 2013; Sun et al., 2016b), so we assumed that emitted Hg conserves the odd

363 isotope MIF of source materials. The Δ^{199}Hg values for most of the $Hg_{PM2.5}$ samples

364 are distinguishable from those of source materials, indicating that anthropogenic

365 emissions were not the drive factors for odd-MIF of $Hg_{PM2.5}$ in the study region. As

366 for MDF, the above analyses indicated that the MDF of $Hg_{PM2.5}$ at the CX was

367 subjected to local anthropogenic sources, while the MDF at the DMS was probably

368 caused by the combination of atmospheric transformations and regional emissions.

369 The result was supported by the correlation between $\delta^{202}Hg$ values and $Hg_{PM2.5}$

370 concentrations which was insignificant at the DMS, but significant at a loose level at

371 the CX (Fig. 3a). Pearson correlation between $\delta^{202}Hg$ and chemical components was

372 further conducted to explore the impacts of anthropogenic emissions on $Hg_{PM2.5}$.

373 The $\delta^{202}Hg$ values at the CX were significantly correlated to Cl^- content ($R^2 =$

374 0.46, $P < 0.05$, Fig. 3b) and well associated with SO_4^{2-} content in $PM_{2.5}$ ($R^2 = 0.38$, P

375 $= 0.056$, Fig. 3c). In this study, Cl^- was mainly originated from coal combustion,

376 given that Cl^- content in $PM_{2.5}$ was not correlated to Na^+. Besides, SO_4^{2-} was

377 primarily transformed from SO_2 which is mainly emitted from coal combustion. The

378 results imply that coal combustion played an important role in the MDF of $Hg_{PM2.5}$ at

379 the CX. It has also been reported that coal combustion has a large contribution of

380 ~50% to total Hg emissions in Zhejiang province (Zhang et al., 2015). Differently

381 from the CX, the $\delta^{202}Hg$ values at the DMS were significantly correlated to SO_4^{2-} (R^2

382 $= 0.68$, $P < 0.05$, Fig. 3c), but not to Cl^- ($P > 0.05$, Table S4). It seems unlikely that

383 coal combustion was the predominant contributor to the positive MDF at the DMS.

384 Whereas under the influence of transport, the transformation of SO_2 to SO_4^{2-} usually

385 enhances and the photo-reduction of Hg^{2+} in aerosols tends to extensive which would

386 shift $\delta^{202}Hg$ to positive to a certain extent (Bergquist and Blum, 2007). The results

387 imply that coal combustion emissions at a regional scale or from long-range transport

388 had a potential impact on the MDF of $Hg_{PM2.5}$ at the DMS, which is consistent with an

389 earlier study conducted at the same site based on Hg concentration and trajectory

390 analysis (Yu et al., 2015).

391 It should be noted that the $\delta^{202}Hg$ values at the CX slightly shift to positive

392 compared to those for emitted Hg_{PM} from coal combustion. Hg isotopic compositions

393 of coals in China have large variations in MDF with $\delta^{202}Hg$ values from -2.36‰ to

394 -0.14‰ (Biswas et al., 2008; Yin et al., 2014b). A prior study estimated that emitted

395 Hg_{PM} has a shift of -0.5‰ relative to $\delta^{202}Hg$ of coal feeds based on the mass balance

396   model (Sun et al., 2014). Then δ^{202}Hg values for Hg$_{PM}$ emitted from coal combustion

397   in China were estimated to be -2.86‰ to -0.64‰. There are many metal smelting

398   factories near the CX. Although we did not measure the tracers for smelting, the mean

399   δ^{202}Hg value for non-ferrous metal ores was reported to be -0.47 ± 0.77‰ (Yin et al.,

400   2016). We assumed that Hg emitted from non-ferrous metal smelting conserves the

401   isotopes of source materials due to a lack of data for processing at the current stage

402   (Sun et al., 2016b). Then, less negative MDF of Hg from non-ferrous metal smelting

403   could explain the positive-shift MDF at the CX relative to coal combustion emissions.

404   Thus, it is reasonably inferred that the MDF of Hg$_{PM2.5}$ at the CX is a result of

405   multiple anthropogenic sources such as coal combustion and non-ferrous metal

406   smelting. In addition, we found a close negative correlation between δ^{202}Hg and

407   levoglucosan content in PM$_{2.5}$ at the CX (R^2 = 0.67, P < 0.05, Fig. 3d) excluding a

408   PM$_{2.5}$ sample collected on Dec. 19, 2017. Levoglucosan is considered an excellent

409   indicative of biomass burning. Thus, we cannot rule out the possibility that the

410   contribution of biomass burning led to a negative deviation of δ^{202}Hg values at the CX

411   to some extent. Previous studies have reported that biological materials display

412   negative δ^{202}Hg and Δ^{199}Hg values, like foliage (δ^{202}Hg: -2.67‰ to -1.79‰; Δ^{199}Hg:

413   -0.47‰ to -0.06‰), litterfall samples (δ^{202}Hg: -3.03‰ to -2.35‰; Δ^{199}Hg: -0.44‰ to

414   -0.22‰), and lichen (δ^{202}Hg: -2.32‰ to -1.83‰; Δ^{199}Hg: -0.35‰ to -0.22‰)

415   (Demers et al., 2013; Jiskra et al., 2015; Yin et al., 2013; Yu et al., 2016; Zheng et al.,

416   2016). Such negative δ^{202}Hg and Δ^{199}Hg of biological materials could not explain the

417   isotopes of Hg$_{PM2.5}$ in this study. Moreover, the contribution of biomass burning is

418   supposed to shift Δ^{199}Hg values negatively, but we found no significant negative

419   correlation between Δ^{199}Hg and K$^+$ or levoglucosan from the whole study period

420   (Table S4). This unexpected result might be due to the fact that the substantial

421   biomass burning often occurs in a short time (i.e., Mar. 2018, Fig. S2a,

422   *https://firms.modaps.eosdis.nasa.gov/*). In this study, the most negative odd-MIF was

423   observed for PM$_{2.5}$ samples collected on Mar. 21, 2018, with a Δ^{199}Hg value of

424   -0.17‰ at the CX and -0.22‰ at the DMS. Those PM$_{2.5}$ samples were likely related

425   to biomass burning, since they were associated with air masses originating from or

passing through the northeast of China with dense fire spots (Fig. S2b). The findings suggest the biomass burning was not the dominant contributor of $Hg_{PM2.5}$ in the study region, but it would change the isotopes of $Hg_{PM2.5}$ in some times.
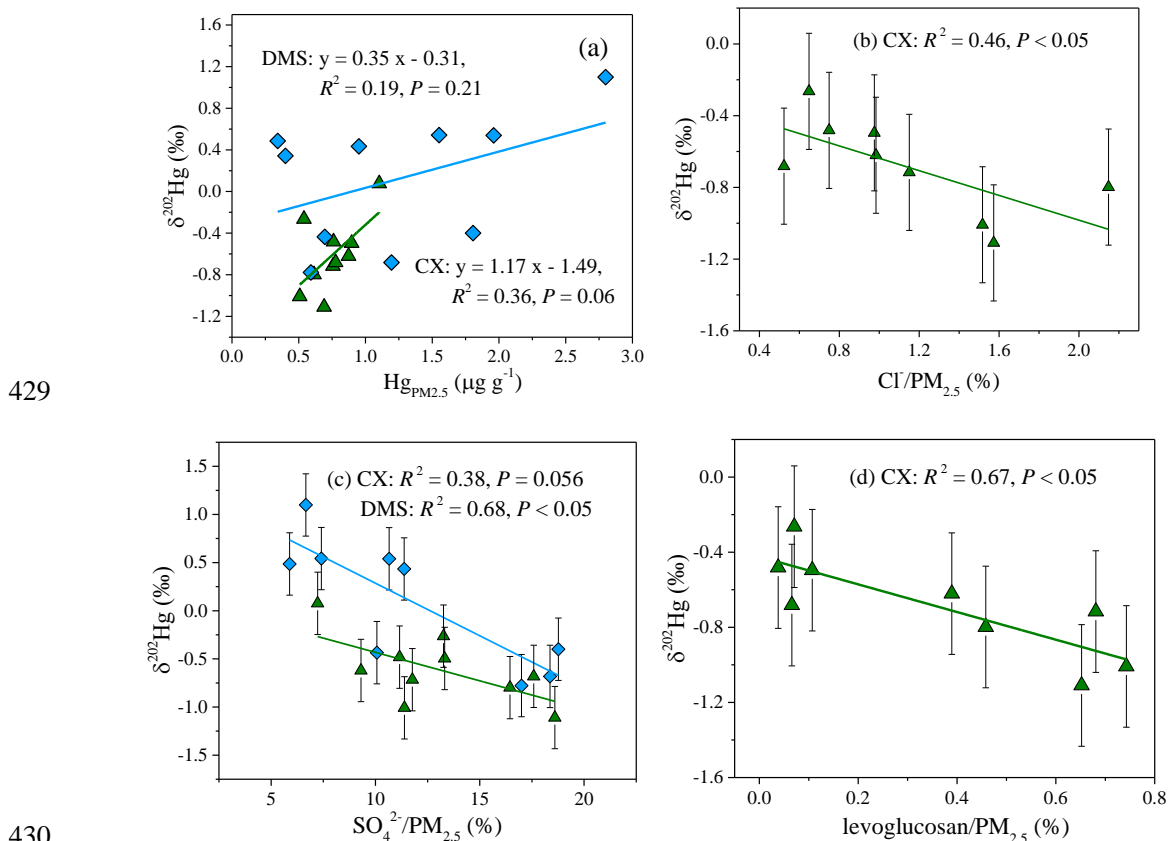
Fig. 3 Relationships of $\delta^{202}Hg$ with (a)Hg, (b) Cl^-, (c) SO_4^{2-}, and (d) levoglucosan contents in $PM_{2.5}$ at CX (▲) or DMS (◆). Uncertainty (2σ) for $\delta^{202}Hg$ in $PM_{2.5}$ is 0.25‰.

3.3. Influence of photo-chemical processes on isotopes of $Hg_{PM2.5}$

Large odd-MIF of Hg isotopes in most $PM_{2.5}$ samples of this study was likely related to photo-chemical processes. An experiment study has found that the oxidation of Hg^0 by halogen atoms (Cl· or Br·) results in a negative shift of $\Delta^{199}Hg$ in product Hg^{2+} (Sun et al., 2016a). Given that partitioning of Hg^{2+} between gas and particle phases leads to limited odd-MIF of Hg isotopes (Fu et al., 2019; Wiederhold et al., 2010), the formation of Hg_{PM} via oxidation of Hg^0 and following adsorption on particles could not explain the positive odd-MIF of $Hg_{PM2.5}$ in this study. Previous experiments and field studies have reported that photo-reduction of inorganic Hg^{2+} in the aqueous solution induces odd-MIF of Hg isotopes and results in large positive $\Delta^{199}Hg$ values in reactants (aerosols here, Bergquist and Blum, 2007; Zheng and

445 Hintelmann, 2009). Hence, photo-reduction of Hg^{2+} in aerosols was invoked as a key

446 factor for the odd-MIF of $Hg_{PM2.5}$ in the study region. The linear relationship between

447 $\Delta^{199}Hg$ and $\Delta^{201}Hg$ is often used to identify the odd-MIF processes of Hg isotopes.

448 The slope of $\Delta^{199}Hg$ versus $\Delta^{201}Hg$ yielded from the data of each site was 1.16 (R^2 =

449 0.92) at the CX and 0.63 (R^2 = 0.85) at the DMS, respectively. The data over the two

450 sites defined a straight line with a slope of 0.92 (R^2 = 0.83, P < 0.01; Fig. 4a). The

451 near-unity slope of $\Delta^{199}Hg$ versus $\Delta^{201}Hg$ was widely observed in particles from

452 coastal site and from other locations in Asia (Fu et al., 2019; Rolison et al., 2013;

453 Huang et al., 2016, 2019; Xu et al., 2019). The $\Delta^{199}Hg/\Delta^{201}Hg$ ratios of this study are

454 more consistent with the indicative ratio of aqueous photo-reduction of inorganic Hg^{2+}

455 (~1.0, Bergquist and Blum, 2007; Zheng and Hintelmann, 2009), but different from

456 the ratios of other processes, like photo-oxidation (1.64 by Br· and 1.89 by Cl·, Sun et

457 al., 2016) and photo-demethylation (1.36, Bergquist and Blum, 2007). Therefore, the

458 photo-reduction of Hg^{2+} in aerosols might be the critical factor for the observed

459 positive odd-MIF of $Hg_{PM2.5}$ in the study region.

460 The similarity of odd-MIF anomaly between the CX and DMS suggests the

461 photo-reduction of Hg^{2+} in aerosols was homogeneous at a regional scale. However,

462 the relationships of $\Delta^{199}Hg$ with $Hg_{PM2.5}$ content and $\delta^{202}Hg$ showed distinct spatial

463 differences. For the DMS, the $\Delta^{199}Hg$ values generally decreased with $Hg_{PM2.5}$ content

464 increased (Fig. 4b) and the correlation between $\Delta^{199}Hg$ and $\delta^{202}Hg$ was significantly

465 positive (R^2 = 0.56, P < 0.05; Fig. 4c). Experimental studies indicated that

466 photo-reduction of Hg^{2+} releases Hg^0 and preferentially retains odd and heavier

467 isotopes in solutions (Bergquist and Blum, 2007; Zheng and Hintelmann, 2009),

468 which is expected to result in a positive relationship between $\Delta^{199}Hg$ and $\delta^{202}Hg$ and

469 an inverse relationship between $\Delta^{199}Hg$ and $Hg_{PM2.5}$ content. In this study, the

470 consistent relationships of $\Delta^{199}Hg$ with $\delta^{202}Hg$ and $Hg_{PM2.5}$ at the DMS strongly imply

471 a predominant role of photo-reduction of Hg^{2+} in isotopic fractionation of $Hg_{PM2.5}$ at

472 this site. Meanwhile, the $\delta^{202}Hg$ signatures of anthropogenic emissions from regional

473 and long-range transport might be largely obscured by photo-reduction process, which

474 well explains the positive $\delta^{202}Hg$ at the DMS. In contrast, the variation of $\Delta^{199}Hg$ at

the CX was not associated with $Hg_{PM2.5}$ contents or $\delta^{202}Hg$. The result suggests an insignificant impact of photo-reduction of Hg^{2+} relative to anthropogenic sources on the MDF and Hg content in $PM_{2.5}$ at the CX.
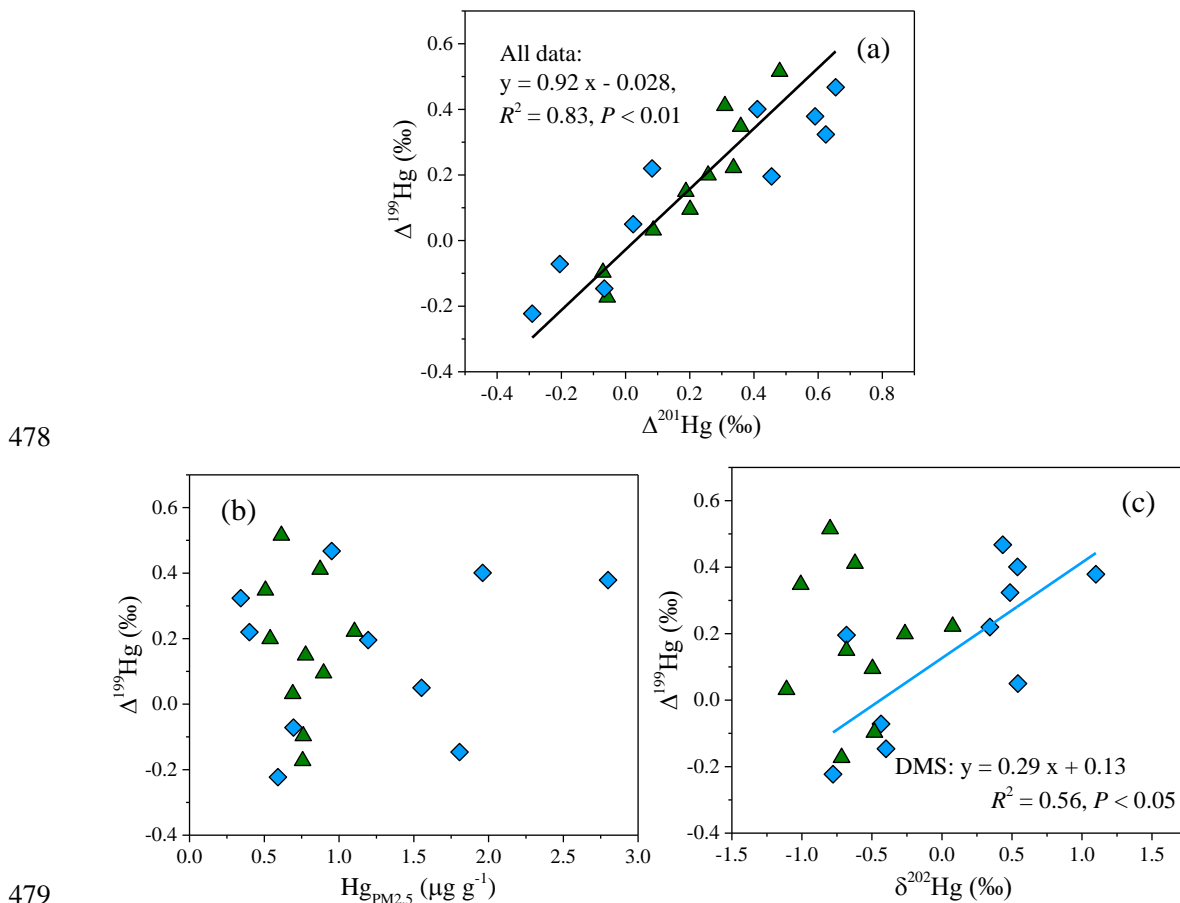
Fig. 4 Linear relationships between (a) $\Delta^{199}Hg$ and $\Delta^{201}Hg$, (b) $\Delta^{199}Hg$ and $Hg_{PM2.5}$ content, and (c) $\Delta^{199}Hg$ and $\delta^{202}Hg$ at the CX (▲) and DMS (◆). Uncertainty (2σ) for $\Delta^{199}Hg$ and $\delta^{202}Hg$ in $PM_{2.5}$ is 0.03‰ and 0.25‰, respectively.

3.4. Potential mechanism of even-MIF

A small but significant MIF of ^{200}Hg was observed in most $PM_{2.5}$ samples from this study, with mean $\Delta^{200}Hg$ values of 0.11 ± 0.07‰ at the CX and 0.14 ± 0.07‰ at the DMS. They are more positive than those in urban (mean = 0.01‰ to 0.09‰, Das et al., 2016; Huang et al., 2016; Xu et al., 2017) and remote areas (mean = 0.07‰ to 0.10‰, Fu et al., 2019), but similar to those in coastal areas and island (Fu et al., 2019; Rolison et al., 2013). In general, Hg emitted from anthropogenic sources has $\Delta^{200}Hg$ of near-zero (Sun et al., 2016b), while large $\Delta^{200}Hg$ values are mainly observed in atmospheric samples, i.e., precipitation, gaseous Hg^{2+}, and aerosols (Chen et al., 2012; Fu et al., 2019; Rolison et al., 2013). Significant even-MIF of Hg isotopes has been

493   suggested to associate with photo-oxidation of Hg^0, from upper troposphere or/and

494   from in situ involving UV light and oxidants (Chen et al., 2012; Fu et al., 2019). This

495   could help explain significant $\Delta^{200}Hg$ values in coastal areas where halogen atoms are

496   expected to be abundant. The $\Delta^{200}Hg$ values in PM$_{2.5}$ were not different between sites,

497   similar to $\Delta^{199}Hg$ values, which supports that the observed $\Delta^{200}Hg$ were associated

498   with photo-chemical processes of minor spatial difference.

499   Gaseous elemental Hg is the predominant form of Hg in atmosphere, which in

500   China was generally characterized by slight negative even-MIF and odd-MIF (Fu et

501   al., 2018; Yu et al., 2020). Given that gas-particle partitioning of Hg^{2+} is strongly

502   temperature-dependent, this process unlikely produces the MIF of Hg isotopes (Fu et

503   al., 2019). Thus, comparing the MIF of Hg isotopes between Hg^0 and Hg$_{PM}$ might

504   shed light on the effect of species conversion on Hg isotopes. The experimental study

505   showed that the oxidation of Hg^0 vapor by Cl· or Br· results in positive $\Delta^{200}Hg$ values

506   in products (Sun et al., 2016a). Thus, this process, which generally enhances in the

507   coastal environment with abundant halogen atoms (Wang et al., 2019), would well

508   explain for the detectable positive $\Delta^{200}Hg$ values in products. However, the oxidation

509   of Hg^0 by Cl· or Br· should produce a negative odd-MIF in products (Sun et al.,

510   2016a), which is inconsistent with the observed positive $\Delta^{199}Hg$ in PM$_{2.5}$. A recent

511   study has reported that oxidation of Hg^0 by oxidizers other than Cl· or Br· might

512   induce a positive odd-MIF in the Hg^{2+}, but this deduction lied on limit isotopic study

513   of Hg^0 oxidation (Yu et al., 2020). Alternatively, the magnitude of photo-reduction of

514   Hg^{2+} larger than the oxidation of Hg^0 by Cl and Br atoms could result in the observed

515   positive odd-MIF of Hg$_{PM}$. Since photo-reduction of Hg^{2+} most likely occurred in

516   aerosols as previously discussed, oxidation of Hg^0 and consequent photo-reduction of

517   Hg^{2+} in aerosols was the possible cause of the positive $\Delta^{199}Hg$ and $\Delta^{200}Hg$ values of

518   PM$_{2.5}$ in the study region.

519   *3.5. Isotopes of Hg in adjacent surface seawater*

520   Hg isotopes are often used to track the transport and transformations of Hg in the

521   environment. The average concentration of THg in seawater was 10.5 $\pm$ 5.0 ng L^{-1},

522   with a range of 1.9 ~ 23.6 ng L^{-1} (Table S1). As shown in Fig. 5, the concentrations of

523   seawater THg displayed distinct time variations, with higher levels during Sep. ~ Mar.

524   than during Apr. ~ Aug, which is likely related to the precipitation cycle. The average

525   δ^{202}Hg value of seawater samples was -1.31 $\pm$ 0.59‰, with most samples fell in the

526   range of -2.00‰ ~ -1.00‰. Whereas the MIF of Hg isotopes in seawater samples was

527   not significant, with mean Δ^{199}Hg, Δ^{201}Hg, and Δ^{200}Hg values of -0.02 $\pm$ 0.07‰, 0.00

528   $\pm$ 0.05‰, and 0.04 $\pm$ 0.03‰, respectively. The negative MDF and near-zero MIF of

529   surface seawater are well consistent with those of source materials (Huang et al., 2016;

530   Sun et al., 2016b), suggesting the dominant effect of anthropogenic emissions on Hg

531   in offshore surface seawater. A minor change in the intensity of industrial activities as

532   expected among the months also supports the above deduction.

533   Isotopic compositions of THg in surface seawater and Hg$_{PM}$ at the adjacent

534   industrial site are consistent in MDF but not in MIF. Similar results were obtained

535   comparing to wet deposition which presented negative δ^{202}Hg and positive Δ^{199}Hg

536   and Δ^{200}Hg values (Chen et al., 2012; Huang et al., 2018). The negative MDF of Hg in

537   industrial PM$_{2.5}$ and adjacent surface seawater implies an important contribution of

538   local anthropogenic sources. On the other hand, the unity slope of Δ^{199}Hg versus

539   Δ^{201}Hg (Δ^{199}Hg = 1.12 $\times$ Δ^{201}Hg - 0.02, R^2 = 0.68, n = 19, Fig. S3) indicates that the

540   odd-MIF of Hg isotopes in surface seawater was mainly produced by photo-reduction

541   of Hg^{2+}. Whereas, the minor Δ^{199}Hg anomalies suggest that photo-reduction was not

542   evident for surface seawater. A big discrepancy in the MIF of Hg isotopes between

543   atmospheric samples and surface seawater further evidences that atmospheric

544   transformations would induce the significant MIF of Hg isotopes and obscure the Hg

545   isotopic signatures of anthropogenic emissions.
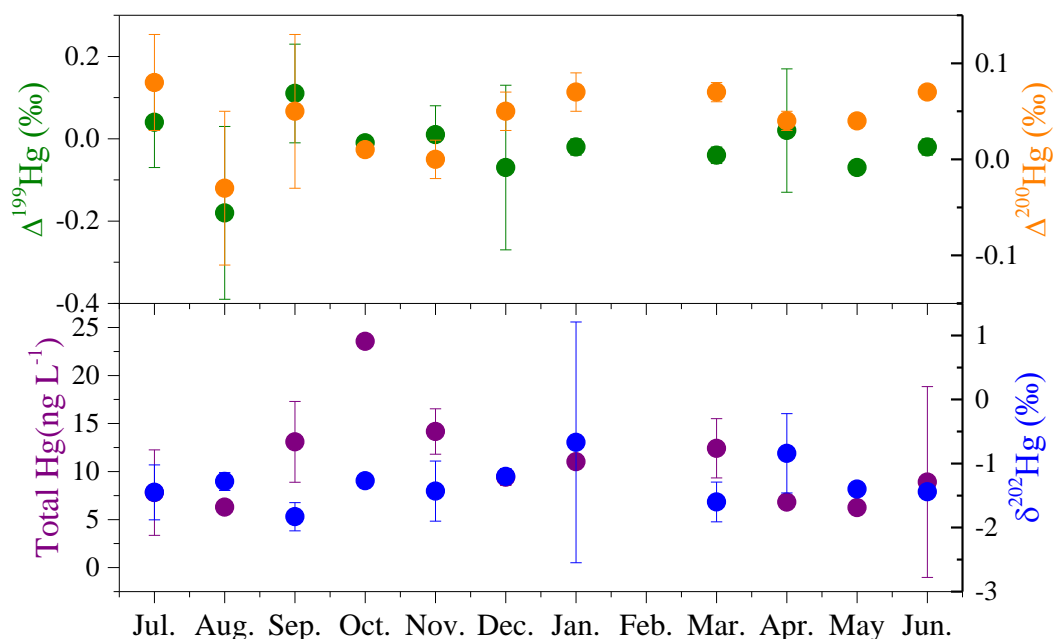
Fig. 5 Monthly variations of total Hg concentration, δ^{202}Hg, Δ^{199}Hg and Δ^{200}Hg of surface seawater during the sampling period from July 2017 to June 2018

4. Conclusion

This study investigated Hg isotopic compositions in PM$_{2.5}$ collected from the neighboring industrial and mountain sites in a coastal area and in surface seawater close to the industrial area. Hg$_{PM2.5}$ displayed a significant spatial difference in MDF but not in odd-MIF. Negative δ^{202}Hg in PM$_{2.5}$ at the CX was primarily induced by local industrial activities like coal combustion. Whereas, the slight positive δ^{202}Hg at the DMS could not be fully explained by anthropogenic emissions. Other than the effect of regional transport, a close correlation between δ^{202}Hg and Δ^{199}Hg at the DMS implies that photo-chemical processes likely contributed to the MDF of Hg$_{PM2.5}$. Significant positive odd-MIF of Hg$_{PM2.5}$ and the unity slope of Δ^{199}Hg versus Δ^{201}Hg indicate an important role of photo-reduction of Hg^{2+} in aerosols. The observed positive Δ^{200}Hg values in this study were probably associated with photo-oxidation of Hg^{0} which is generally enhanced in the coastal environment. THg in surface seawater was characterized by negative MDF and near-zero odd-MIF, which is more consistent with isotopic signatures of source materials. The MIF anomalies of Hg isotopes were larger for atmospheric PM$_{2.5}$ than for surface seawater, suggesting that atmospheric transformations induce significant MIF of Hg isotopes and obscure Hg isotopic signatures of initial anthropogenic emissions.

Novelty statement

A comparison of isotopic compositions of Hg$_{PM2.5}$ was conducted between the neighboring industrial and mountain sites, which effectively revealed the influence of anthropogenic emission sources and transformation processes on Hg isotopes. Hg isotopic compositions in industrial PM$_{2.5}$ and offshore surface seawater were also compared. The results indicate that atmospheric transformations would induce significant fractionation of Hg isotopes and obscure specific Hg isotopic signatures of initial emissions.

Data availability. HYSPLIT trajectory model and gridded meteorological data (Global Data Assimilation System, GDAS1) are available from the US National Oceanic and Atmospheric Administration (http://ready.arl.noaa.gov). Fire data are available in the Fire Information for Resource Management System (FIRMS, https://firms2.modaps.eosdis.nasa.gov/map/#d:2021-04-26..2021-04-27;@6.7,2.0,3z). All data in this study are available upon request to the first author via email (linglingxu@iue.ac.cn).

Author contributions. JSC, LLX, and YRZ designed this study. MRL, LQY, YTC, LT and HX conducted the sampling. YRZ and LLX participated in sample treatment and measurements. LLX wrote the paper. JYS and YPC helped the graphics production. All authors reviewed the paper.

Competing interests. The authors declare that they have no conflict of interest.

Acknowledgements. This research was financially supported by National Natural Science Foundation of China (No. 21507127; 41575146 & U1405235), Natural Science Foundation of Fujian province (2016J05050), the Cultivating Project of Strategic Priority Research Program of Chinese Academy of Sciences (XDPB1903), the CAS Center for Excellence in Regional Atmospheric Environment (E0L1B20201), and Xiamen Atmospheric Environment Observation and Research Station of Fujian

597 Province. We would like to thank Shuyuan Huang (Xiamen University) for his help in
598 Hg isotopes analysis. We also thank the handling editor and two reviewers for their
599 constructive comments and suggestions.
600

601 **References**

602 Bergquist, B. A. and Blum, J. D.: Mass-dependent and -independent fractionation of
603   Hg isotopes by photoreduction in aquatic systems, Science, 318, 417–420, doi:
604   10.1126/science.1148050, 2007.

605 Biswas, A., Blum, J. D., Bergquist, B. A., Keeler, G. J., Xie, Z. Q.: Natural mercury
606   isotope variation in coal deposits and organic soils, Environ. Sci. Technol.,
607   42(22), 8303−8309, doi: 10.1021/es801444b, 2008.

608 Blum, J. D. and Bergquist, R. A.: Reporting of variations in the natural isotopic
609   composition of mercury, Anal. Bioanal. Chem., 338(2), 353–359, doi:
610   org/10.1007/s00216-007-1236-9, 2007.

611 Blum, J. D., Sherman, L. S., Johnson, M. W.: Mercury isotopes in earth and
612   environmental sciences, Annu. Rev. Earth Planet. Sci., 42, 249–269, doi:
613   10.1146/annurev-earth-050212-124107, 2014.

614 Blum, J. D. and Johnson, M. W.: Recent developments in mercury stable isotope
615   analysis, Non-Traditional Stable Isotopes, 82, 733-757, doi:
616   10.2138/rmg.2017.82.17, 2017.

617 Chen, J. B., Hintelmann, H., Feng, X. B., Dimock, B.: Unusual fractionation of both
618   odd and even mercury isotopes in precipitation from Peterborough, ON, Canada,
619   Geochim. Cosmochim. Ac., 90, 33−46, doi: 10.1016/j.gca.2012.05.005, 2012.

620 Das, R., Wang, X. F., Khezri, B., Webster, R. D., Sikdar, P. K., Datta, S.: Mercury
621   isotopes of atmospheric particle bound mercury for source apportionment study
622   in urban Kolkata, India, Elementa-Sci. Anthrop., 4, 1−12, doi: 10.12952/journal.
623   elementa.000098, 2016.

624 Demers, J. D., Blum, J. D., Zak, D. R.: Mercury isotopes in a forested ecosystem:
625   Implications for air-surface exchange dynamics and the global mercury cycle,
626   Global Biogeochem. Cy., 27(1), 222−238, doi: 10.1002/gbc.20021, 2013.

Fu, X. W., Zhang, H., Yu, B., Wang, X., Lin, C.-J., and Feng, X. B.: Observations of atmospheric mercury in China: a critical review, Atmos. Chem. Phys., 15, 9455–9476, doi:10.5194/acp-15-94552015, 2015.

Fu, X. W., Yang, X., Tan, Q. Y., Ming, L. L., Lin, T., Lin, C.-J., Li, X. D., Feng, X. B.: Isotopic composition of gaseous elemental mercury in the marine boundary layer of East China Sea, J. Geophys. Res.: Atmos., 123, 7656–7669, doi: 10.1029/2018JD028671, 2018.

Fu, X. W., Zhang, H., Feng, X. B., Tan, Q. Y., Ming, L. L., Liu, C., Zhang, L. M.: Domestic and transboundary sources of atmospheric particulate bound mercury in remote areas of China: Evidence from mercury isotopes, Environ. Sci. Technol., 53(4), 1947−1957, doi: 10.1021/acs.est.8b06736, 2019.

GMA: Global Mercury Assessment 2018. UN Environment Programme, Chemicals and Health Branch Geneva, Switzerland.

Guo, J. M., Sharma, C. M., Tripathee L., Kang, S. C., Fu, X. W., Huang, J., Shrestha K. L., Chen, P. F.: Source identification of atmospheric particle-bound mercury in the Himalayan foothills through non-isotopic and isotope analyses, Environ. Pollut., 286, 117317, doi: 10.1016/j.envpol.2021.117317, 2021.

Guo, J. M., Tripathee, L., Kang, S. C., Zhang, Q. G., Huang, J., Sharma, C. M., Chen, P. F., Paudyal, R., Rupakheti, D.: Atmospheric particle-bound mercury in the northern Indo-Gangetic Plain region: Insights into sources from mercury isotope analysis and influencing factors, Geosci. Front., 13, 101274, doi: 10.1016/j.gsf.2021.101274, 2022.

Horowitz, H. M., Jacob, D. J., Zhang, Y. X., Dibble, T. S., Slemr, F., Amos, H. M., Schmidt, J. A., Corbitt, E. S., Marais, E. A., Sunderland, E. M.: A new mechanism for atmospheric mercury redox chemistry: implications for the global mercury budget, Atmos. Chem. Phys., 17(10), 6353−6371, doi: org/10.5194/acp-17-6353-2017, 2017.

Hong, Y. W., Chen, J. S., Deng, J. J., Tong, L., Xu, L. L., Niu, Z. C., Yin, L. Q., Chen, Y. T., Hong, Z. Y.: Pattern of atmospheric mercury speciation during episodes of elevated PM2.5 levels in a coastal city in the Yangtze River Delta, China,

Environ. Pollut., 218, 259-268, doi: 10.1016/j.envpol.2016.06.073, 2016.

Hong, Z. Y., Zhang, H., Zhang, Y. R., Xu, L. L., Liu, T. T., Xiao, H., Hong, Y. W., Chen, J. S., Li, M. R., Deng, J. J., Wu, X., Hu, B. Y., Chen, X. Q.: Secondary organic aerosol of PM2.5 in a mountainous forest area in southeastern China: Molecular compositions and tracers implication, Sci, Total Environ. 653: 496−503, doi: 10.1016/j.scitotenv.2018.10.370, 2019.

Huang, Q., Liu, Y. L., Chen, J. B., Feng, X. B., Huang, W. L., Yuan, S. L., Cai, H. M., Fu, X. W.: An improved dual-stage protocol to pre-concentrate mercury from airborne particles for precise isotopic measurement, J. Anal. Atom. Spectrom., 30(4), 957−966, doi: 10.1039/c4ja00438h, 2015.

Huang, Q., Chen, J. B., Huang, W. L., Fu, P. Q., Guinot, B., Feng, X. B., Shang, L. H., Wang, Z. H., Wang, Z. W., Yuan, S. L., Cai, H. M., Wei, L. F., Yu, B.: Isotopic composition for source identification of mercury in atmospheric fine particles, Atmos. Chem. Phys., 16(18), 11773–11786, doi:10.5194/acp-16-11773-2016, 2016.

Huang, S. Y., Sun, L. M., Zhou, T. J., Yuan, D. X., Du, B., Sun, X. W.: Natural stable isotopic compositions of mercury in aerosols and wet precipitations around a coal-fired power plant in Xiamen, southeast China, Atmos. Environ., 173, 72−80, doi: 10.1016/j.atmosenv.2017.11.003, 2018.

Huang, Q., Chen, J. B., Huang, W. L., Reinfelder, J. R., Fu, P. Q., Yuan, S. L., Wang, Z. W., Yuan, W., Cai, H. M., Ren, H., Sun, Y. L., He, L.: Diel variation in mercury stable isotope ratios records photoreduction of PM2.5-bound mercury, Atmos. Chem. Phys., 19(1), 315−325, doi: 10.5194/acp-19-315-2019, 2019.

Huang, Q., Reinfelder, J. R., Fu, P. Q., Huang, W. L.: Variation in the mercury concentration and stable isotope composition of atmospheric total suspended particles in Beijing, China, J. Hazard. Mater., 383, 121131, doi: 10.1016/j.jhazmat. 2019.121131, 2020.

Huang, S. Y., Zhao, Y. H., Lv, S. P., Wang, W. G., Wang, W. L., Zhang, Y. B., Huo, Y. L., Sun, X. W., Chen, Y. J.: Distribution of mercury isotope signatures in Yundang Lagoon, Xiamen, China, after long-term interventions, Chemosphere,

272, 129716, doi: 10.1016/j.chemosphere.2021.129716, 2021.

Jiskra, M., Wiederhold, J. G., Skyllberg, U., Kronberg, R. M., Hajdas, I., Kretzschmar, R.: Mercury deposition and re-emission pathways in boreal forest soils investigated with Hg isotope signatures, Environ. Sci. Technol., 49(12), 7188−7196, doi: 10.1021/acs.est.5b00742, 2015.

Lin, H. Y., Yuan, D. X., Lu, B. Y., Huang, S. Y., Sun, L. M., Zhang, F., Gao, Y. Q.: Isotopic composition analysis of dissolved mercury in seawater with purge and trap preconcentration and a modified Hg introduction device for MC-ICP-MS, J. Anal. Atom. Spectrom., 30(2), 353−359, doi: 10.1039/c4ja00242c, 2015.

Malinovsky, D., Latruwe, K., Moens, L., Vanhaecke, F.: Experimental study of mass-independence of Hg isotope fractionation during photodecomposition of dissolved methylmercury, J. Anal. Atom. Spectrom., 25(7), 950-956, doi: 10.1039/b926650j, 2010.

Mao, H. T., Cheng, I., Zhang, L. M.: Current understanding of the driving mechanisms for spatiotemporal variations of atmospheric speciated mercury: a review, Atmos. Chem. Phys., 16(20), 12897-12924, doi: 10.5194/acp-16-12897-2016, 2016.

Rolison, J. M., Landing, W. M., Luke, W., Cohen, M., Salters, V. J. M.: Isotopic composition of species-specific atmospheric Hg in a coastal environment, Chem. Geol., 336, 37−49, doi: 10.1016/j.chemgeo.2012.10.007, 2013.

Schroeder, W. H. and Munthe J.: Atmospheric mercury—An overview, Atmos. Environ., 32(5), 809–822, doi:10.1016/S1352-2310(97) 00293-8, 1998.

Schleicher, N. J., Schäfer, J., Blanc, G., Chen, Y., Chai, F., Cen, K., Norra, S.: Atmospheric particulate mercury in the megacity Beijing: spatio-temporal variations and source apportionment, Atmos. Environ., 109, 251–261, doi: 10.1016/j.atmosenv.2015.03.018, 2015.

Selin, N. E.: Global biogeochemical cycling of mercury: A review, Annu. Rev. Env. Resour., 34, 43–63, doi: 10.1146/annurev.environ.051308.084314, 2009.

Sonke, J. E. and Blum, J. D.: Advances in mercury stable isotope biogeochemistry preface, Chem. Geol., 336, 1–4, doi: 10.1016/j.chemgeo.2012.10.035, 2013.

Sun, R. Y., Heimburger, L. E., Sonke, J. E., Liu, G. J.: Mercury stable isotope fractionation in six utility boilers of two large coal-fired power plants, Chem. Geol., 336, 103−111, doi: 10.1016/j.chemgeo.2012.10.055, 2013.

Sun, R. Y., Sonke, J. E., Heimburger, L. E., Belkin, H. E., Liu, G. J., Shome, D., Cukrowska, E., Liousse, C., Pokrovsky, O. S., Streets, D. G.: Mercury stable isotope signatures of world coal deposits and historical coal combustion emissions, Environ. Sci. Technol., 48(13), 7660−7668, doi: 10.1021/es501208a, 2014.

Sun, G. Y., Sommar, J., Feng, X. B., Lin, C.-J., Ge, M. F., Wang, W. G., Yin, R. S., Fu, X. W., Shang, L. H.: Mass-dependent and -independent fractionation of mercury isotope during gas-phase oxidation of elemental mercury vapor by atomic Cl and Br, Environ. Sci. Telchnol., 50(17), 9232−9241, doi: 10.1021/acs.est.6b01668, 2016a.

Sun, R. Y., Streets, D. G., Horowitz, H. M., Amos, H. M., Liu, G. J., Perrot, V., Toutain, J.P., Hintelmann, H., Sunderland, E. M., Sonke, J. E.: Historical (1850-2010) mercury stable isotope inventory from anthropogenic sources to the atmosphere, Elementa-Sci. Anthrop., 4, 1−15, doi: 10.12952/journal.elementa.000091, 2016b.

Wang, S. Y., McNamara, S. M., Moore, C. W., Obrist, D., Steffen, A., Shepson, P. B., Steabler, R. M., Raso, A. R. W., Pratt, K. A.: Direct detection of atmospheric atomic bromine leading to mercury and ozone depletion, P. Natl. Acad. Sci., 116(29), 14479−14484, doi: 10.1073/pnas.1900613116, 2019.

Wiederhold, J. G.; Cramer, C. J.; Daniel, K.; Infante, I.; Bourdon, B.; Kretzschmar, R.: Equilibrium mercury isotope fractionation between dissolved Hg(II) species and thiol-bound Hg, Environ. Sci. Technol., 44 (11), 4191−4197, doi: 10.1021/es100205t, 2010.

Xu, L. L., Chen, J. S., Yang, L. M., Yin, L. Q., Yu, J. S., Qiu, T. X., Hong, Y.W.: Characteristics of total and methyl mercury in wet deposition in a coastal city, Xiamen, China: Concentrations, fluxes and influencing factors on Hg distribution in precipitation, Atmos. Environ. 99, 10−16, doi: 10.1016/j.atmosenv.2014.09.054, 2014.

Xu, H. M., Sonke, J. E., Guinot, B., Fu, X. W., Sun, R. Y., Lanzanova, A., Candaudap, F., Shen, Z. X., Cao, J. J.: Seasonal and annual variations in atmospheric Hg and Pb isotopes in Xi'an, China, Environ. Sci. Technol., 51(7), 3759−3766, doi: 10.1021/acs.est.6b06145, 2017.

Xu, L. L., Jiao, L., Hong, Z. Y., Zhang, Y. R., Du, W. J., Wu, X., Chen, Y. T., Deng, J. J., Hong, Y. W., Chen, J. S.: Source identification of $PM_{2.5}$ at a port and an adjacent urban site in a coastal city of China: Impact of ship emissions and port activities, Sci. Total Environ., 634: 1205 − 1213, doi: 10.1016/j.scitotenv.2018.04.087, 2018.

Xu, H. M., Sun, R. Y., Cao, J. J., Huang, R. J., Guinot, B., Shen, Z. X., Jiskra, M., Li, C. X., Du, B. Y., He, C., Liu, S.X., Zhang, T., Sonke, J. E.: Mercury stable isotope compositions of Chinese urban fine particulates in winter haze days: Implications for Hg sources and transformations, Chem. Geol., 504, 267−275, doi: 10.1016/j.chemgeo.2018.11.018, 2019.

Xu, L. L., Zhang, Y. R., Tong, L., Chen, Y. P., Zhao, G. Q., Hong, Y. W., Xiao, H., Chen, J. S.: Gas-particle partitioning of atmospheric reactive mercury and its contribution to particle bound mercury in a coastal city of the Yangtze River Delta, China, Atmos. Environ., 239, 117744, doi: 10.1016/j.atmosenv.2020.117744, 2020.

Yin, R. S., Feng, X. B., Meng, B.: Stable mercury isotope variation in rice plants (Oryza sativa L.) from the Wanshan mercury mining district, SW China, Environ. Sci. Technol., 47(5), 2238−2245, doi: 10.1021/es304302a, 2013.

Yin, R. S., Feng, X. B., Li, X. D., Yu, B., Du, B. Y.: Trends and advances in mercury stable isotopes as a geochemical tracer, Trends Environ. Anal., 2, 1−10, doi: 10.1021/es500322n, 2014a.

Yin, R. S., Feng, X. B., Chen, J. B.: Mercury stable isotopic compositions in coals from major coal producing fields in China and their geochemical and environmental Implications, Environ. Sci. Technol., 48(10), 5565−5574, doi: 10.1021/es500322n, 2014b.

776 Yin, R. S., Feng, X. B., Hurley, J. P., Krabbenhoft, D. P., Lepak, R. F., Hu, R. Z.,
777   Zhang, Q., Li, Z. G., Bi, X. W.: Mercury isotopes as proxies to identify sources
778   and environmental impacts of mercury in Sphalerites, Sci. Rep., 6, 2045−2322,
779   doi: 10.1038/srep18686, 2016.

780 Yu, B., Wang, X., Lin, C. J., Fu, X. W., Zhang, H., Shang, L. H., Feng, X. B.:
781   Characteristics and potential sources of atmospheric mercury at a subtropical
782   near-coastal site in East China, J. Geophys. Res.-Atmospheres, 120(16),
783   8563−8574, doi:10.1002/2015JD023425, 2015.

784 Yu, B., Fu, X. W., Yin, R. S., Zhang, H., Wang, X., Lin, C. J., Wu, C. S., Zhang, Y. P.,
785   He, N. N., Fu, P. Q., Wang, Z. F., Shang, L. H., Sommar, J., Sonke, J. E.,
786   Maurice, L., Guinot, B., Feng, X. B.: Isotopic composition of atmospheric
787   mercury in China: New evidence for sources and transformation processes in air
788   and in vegetation, Environ. Sci. Technol., 50(17), 9262−9269, doi:
789   10.1021/acs.est.6b01782, 2016.

790 Yu, B., Yang, L., Wang, L. L., Liu, H. W., Xiao, C. L., Ling, Y., Liu, Q., Yin, Y. G., Hu,
791   L. G., Shi, J. B., Jiang, G. B.: New evidence for atmospheric mercury
792   transformations in the marine boundary layer from stable mercury isotopes,
793   Atmos. Chem. Phys., 20, 9713−9723, doi: 10.5194/acp-20-9713-2020, 2020.

794 Zhang, L., Wang, S. X., Wang, L., Wu, L., Duan, L., Wu, Q. R., Wang, F. Y., Yang, M.,
795   Yang, H., Hao, J. M., Liu, X.: Updated emission inventories for speciated
796   atmospheric mercury from anthropogenic sources in China, Environ. Sci.
797   Technol., 49(5), 3185−3194, doi: 10.1021/es504840m, 2015.

798 Zheng, W. and Hintelmann, H.: Mercury isotope fractionation during photoreduction
799   in natural water is controlled by its Hg /DOC ratio, Geochim. Cosmochim. Ac.,
800   73, 6704−6715, doi: 10.1016/j.gca.2009.08.016, 2009.

801 Zheng, W., Obrist, D., Weis, D., Bergquist, B. A.: Mercury isotope compositions
802   across North American forests, Global Biogeochem. Cy., 30(10), 1475−1492, doi:
803   10.1002/2015gb005323, 2016.